Temporal shaping of single photons by engineering exciton dynamics in a single quantum dot

View Online   Export Citation   CrossMark

Kyu-Young Kim,[1] Christopher J. K. Richardson,[2] (iD) Edo Waks,[3,4] (iD) and Je-Hyung Kim[1,a] (iD)

AFFILIATIONS

[1] Department of Physics, Ulsan National Institute of Science and Technology, Ulsan 44919, Republic of Korea
[2] Laboratory for Physical Sciences, University of Maryland, College Park, Maryland 20740, USA
[3] Department of Electrical and Computer Engineering and Institute for Research in Electronics and Applied Physics, University of Maryland, College Park, Maryland 20742, USA
[4] Joint Quantum Institute, University of Maryland and the National Institute of Standards and Technology, College Park, Maryland 20742, USA

Note: This paper is part of the APL Photonics Special Topic on Integrated Quantum Photonics.
[a] Author to whom correspondence should be addressed: jehyungkim@unist.ac.kr

ABSTRACT

The majority of photonic quantum information technologies rely on single photons that have high purity and indistinguishability. Although solid-state quantum emitters can serve such single photons on demand, their asymmetric temporal and spatial mode profiles limit the optimal efficiency and fidelity of quantum interaction. Here, we demonstrate single-photon pulses at a telecom wavelength with a Gaussian-like temporal mode profile from a cavity-coupled single quantum dot. Engineering the exciton dynamics via multi-exciton cascade recombination and cavity detuning enables us to modify the rise and decay dynamics of single excitons. Furthermore, the cascade recombination process temporally retards the single-exciton emission from the background emission, leading to possible purification of single photons at high excitation power. In addition, coupling quantum dots into a low Q cavity mode leads to a Gaussian-like spatial mode profile, which brings a high collection efficiency. This approach paves the way for producing single photons with an optimized temporal and spatial waveform.

I. INTRODUCTION

Photons are important carriers in quantum information processing with the capability to encode information with their multiple degrees of freedom, such as polarization, time-bins, and spatial modes. Recent advances in photonic technologies for efficient generation, manipulation, and detection of photons enable fascinating quantum applications, such as secured quantum key distribution,[1,2] quantum teleportation,[3] quantum imaging beyond classical diffraction limits,[4] and quantum simulations with high computation powers.[5,6]

Semiconductor quantum dots (QDs) can generate highly indistinguishable single photons and entangled photon pairs with high fidelity.[7–11] In addition, the ability to integrate with micro/nanophotonic structures has enabled high brightness,[12–14]

Purcell enhancement,[15–17] and single-photon nonlinearity.[18,19] Currently, these sources are in the leap forward for scalable and distributed quantum systems involving multiple photons and nodes.[20–22]

In scalable quantum photonic systems, tailoring single photons into proper spatial and temporal profiles, such as Gaussian, becomes much more important for achieving optimal quantum interactions between photon-to-photon or photon-to-atom. The Gaussian spatial mode profile has been demonstrated with various photonic structures, such as nanowires,[13,23] Bull's eyes,[8,24] solid-immersion lenses,[25] and photonic crystal cavities.[26] This Gaussian-like spatial mode is beneficial to maximize the mode overlap between photons and to achieve high coupling efficiency into lenses or optical fibers. The Gaussian temporal profile is also highly desirable because it allows for efficient unitary interactions between qubits and has the

most tolerance in mode mismatching of the temporal mode profile of single photons.[27,28] However, such a temporal profile requires temporally reversible emission and absorption processes, which are inherently difficult in solid-state quantum emitters due to their fast rise time of ps order and slow decay time of ns order.

Several approaches for modifying the temporal profile of the single-photon emission have been proposed by temporally modulating the excitation or emission pulses of quantum emitters. For example, an ns-long excitation pulse can generate a long rise time of single-photon emissions, but the increased re-excitation probability decreases the single-photon purity.[29] Applying an electro-optic modulator can filter the emission pulses into the Gaussian temporal profile with a narrower full width at half maximum (FWHM).[30,31] However, significant photon loss is inevitable for temporal modulation from an asymmetric emission pulse to a Gaussian pulse (see the supplementary material, S1).

Here, we demonstrate a single-photon emission with the Gaussian mode profile in both temporal and spatial domains from the QDs in a photonic crystal cavity. Instead of manipulating the excitation or emission pulses, we directly engineer the exciton dynamics in the QDs to make the emitter produce time-symmetric single-photon emission. To tailor the exciton dynamics, we introduce multi-exciton complexes and their cascade recombination process. This process effectively increases the rise time of a single-exciton state and temporally separates single photons from background emissions. Such temporal separation enables us to recover the purity of single photons at much higher excitation power than the saturation power. Additionally, the integration with an $L3$ photonic crystal cavity shortens the decay time through the Purcell enhancement and modifies the far-field profile, leading to a temporal- and spatial-Gaussian-like single-photon waveform.

II. RESULT

In this study, we used self-assembled InAs/InP QDs integrated with an $L3$-photonic crystal cavity. The QDs are embedded in a 280 nm thick InP matrix on a 2 μm AlInAs sacrificial layer. The density of QDs is ~10 μm^{-2}.[32] Using an electron beam lithography technique followed by a reactive ion etching process, we patterned $L3$ photonic crystal cavities, as shown in Fig. 1(a).

We first examined the emission spectra of the cavity-coupled QDs using a 785 nm pulsed excitation laser at 4 K (see the supplementary material, S2). Figure 1(b) shows measured spectra at low and high excitation power densities of 0.5×10^5 and 4.0×10^6 W/m^2, respectively, with an approximate beam spot size of 1 μm^2. At low excitation power, we observe a bright peak at 1289 nm, near the telecom O-band. The peak corresponds to single-exciton emission verified by power-dependent measurement (see the supplementary material, S3). Increasing the excitation laser power above the saturation power density ($P_0 = 1.0 \times 10^5$ W/m^2) creates a large number of carriers that fill the excited and hybridized continuum states of QDs and a wetting layer.[33,34] These emissions can efficiently feed the cavity mode resonantly and non-resonantly via phonons, resulting in strong cavity mode emissions at high excitation power[35] [bottom of Fig. 1(b)].

The cavity spectrum at high excitation power shows multiple modes M2–M4 of the $L3$ photonic crystal cavity,[35–37] and we
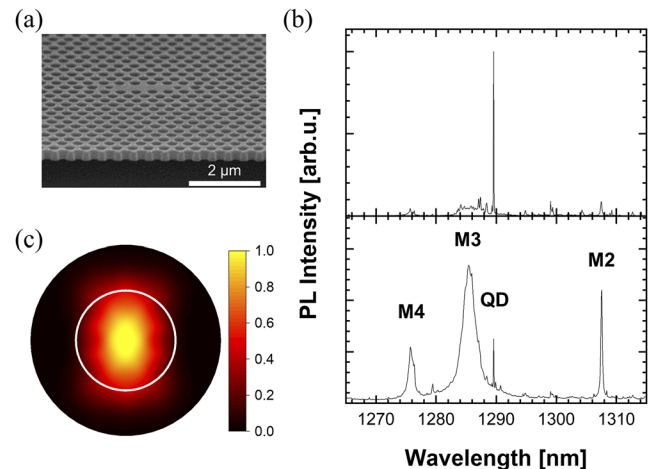

FIG. 1. (a) Tilted view of a scanning electron microscope image of an $L3$ photonic crystal cavity. (b) Low temperature (4 K) PL spectra of the sample at different excitation power densities of $P = 0.5 \times 10^5$ (top) and 4.0×10^6 W/m^2 (bottom). M2–M4 at high excitation power denotes higher-order modes of the $L3$ photonic crystal cavity, and QD denotes a studied QD coupled to M3. (c) Far-field profile $|E|^2$ of the M3 mode of the cavity calculated by finite-difference time-domain simulation. The white circle represents the collection angle $\theta = 44.4°$, corresponding to NA = 0.7 of the objective lens.

choose the single QD coupled to a higher-order mode M3. Compared to other modes, mode M3 has a low Q value around 500 (see the supplementary material, S4). However, mode M3 has a distinctive advantage of vertical emission with a Gaussian-like profile. In the numerical simulation, this mode M3 shows a Gaussian-like far-field pattern [Fig. 1(c)]. Although each axis of the far-field profile is very close to a Gaussian function, the elliptical shape gives the spatial mode overlap integral of 78.7% between the mode M3 and the Gaussian function (see the supplementary material, S5). From this low Q Gaussian-like spatial mode, we calculate the collection efficiency of 43% over the 12 nm spectral range. The efficiency includes the upward and partially reflected downward emissions from the bottom InP layer with a 2 μm air gap within the numerical aperture (NA) of 0.7. Having a high reflectivity bottom mirror can improve the efficiency up to 70%. Therefore, this mode is advantageous to enhance the brightness of QD emissions over a broad spectral range. In the experiment, we determine a collection efficiency of 19(7)% for the single QD in Fig. 1(b) (see the supplementary material, S6). The discrepancy would be due to the spectral and spatial mode mismatch between the QD and M3.

To characterize the exciton dynamics of the cavity-integrated QDs, we performed time-resolved photoluminescence (TRPL) measurements. A 780 nm pulsed laser with an FWHM of 70 ps excited the sample, and InGaAs single-photon detectors with a time-correlated single-photon counter recorded the histograms for TRPL and second-order photon-correlation measurements with a temporal resolution of 200 ps. In Fig. 2(a), we first investigate the exciton dynamics with increasing the excitation power up to $50P_0$ at a 40 MHz excitation laser repetition rate. To characterize the time scales of rise and decay parts of the TRPL curves, we separately fit the curves with a single exponential function. Since the rise time is as
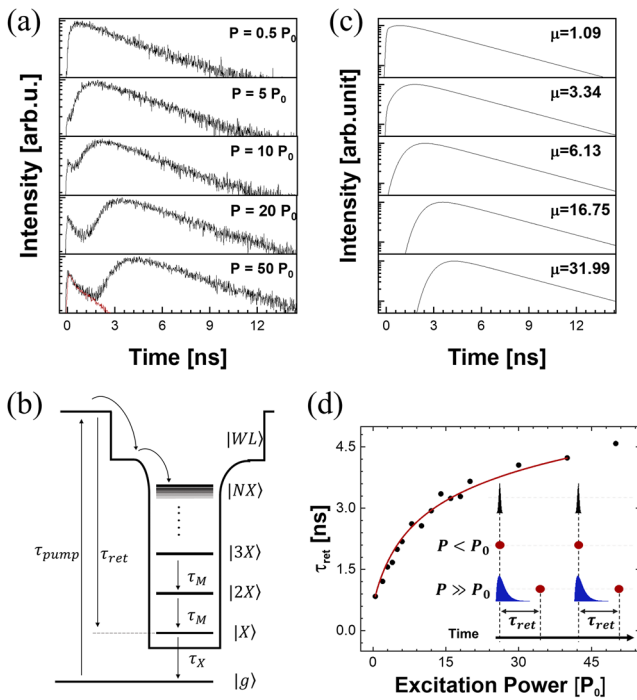
FIG. 2. (a) Measured TRPL curves of a single-exciton state (black lines) with increasing the excitation power at 4 K. A red line at $P = 50P_0$ in (a) represents a measured TRPL curve of the M3 cavity mode for comparison. (b) Schematic of energy level structures in a QD, including multi-exciton states ($|NX\rangle$) and a wetting layer ($|WL\rangle$). Each multi-exciton state has a decay time (τ_M), and this cascade recombination process results in total temporal retardation (τ_{ret}) to the single-exciton state. (c) Calculated TRPL curves using Eq. (1) at various μ from (a). (d) Measured τ_{ret} as a function of single-exciton saturation power density ($P_0 = 1.0 \times 10^5$ W/m^2). A red line is a calculated τ_{ret} curve using Eq. (1). The inset shows a schematic of the laser (black peak), single-exciton emission (I_X, red circle), and cavity emission (I_C, blue curve) with time at low and high excitation powers.

fast as the system temporal resolution around 200 ps, we convolute the fitted curve with an instrument response function. At $P = 0.5P_0$, the single exciton shows a fast rise time of 0.2 ns and a slow decay time of 4.1 ns. As the excitation power increases, first, the rise part of the TRPL curve is noticeably extended to 1.32 ns ($P = 10P_0$) and then starts to temporally shift away from the excitation laser pulse. Meanwhile, the decay time of the single exciton remains almost constant during the power-varying TRPL measurements.

To understand the change in the exciton dynamics with the excitation power, we consider a multi-exciton complex model in a single QD. As described in the schematic in Fig. 2(b), the above-band excitation initially generates the carriers in a host material. At low excitation laser power, these photo-excited carriers are rapidly captured and relaxed into a single-exciton state via phonon interaction and Auger scattering.[38,39] At the above saturation power, the carriers begin to form multi-exciton complexes such as bi-excitons. Since bi-exciton recombination slowly populates the single-exciton state, it delays the rise time of a single-exciton emission. As we increase the excitation power further, a larger number of excitons can be created in the single QD,[33,34,40] and their cascade recombination leads to a

temporal shift of the single-exciton emission, which can be clearly seen above $20P_0$ in Fig. 2(a).

For more quantitative analysis of the exciton dynamics, we follow the model in Refs. 33 and 34, which describes the temporal intensity profile of the single exciton as (see the supplementary material, S7),

$$I_X(t) = e^{-\frac{t}{\tau_X}}\left[\exp\left(-\mu e^{-\frac{t}{\tau_M}}\right)\left(1 + \mu e^{-\frac{t}{\tau_M}}\right) - e^{-\mu}\right]. \quad (1)$$

We consider an averaged decay time τ_M for each multi-exciton state. Through the cascade recombination process, the multi-excitons reach a bi-exciton state and the bi-exciton state feeds the single-exciton state. We determine the decay time of the single-exciton state $\tau_X = 4.1$ ns from the experimental decay time at $P = 0.5P_0$. We also find $\tau_M = 1.1$ ns by fitting the experimental data at high excitation powers (see the supplementary material, S7) and use the value as a fixed constant for all excitation power. μ accounts a mean exciton number following Poisson distribution, and we set it as a fitting parameter for the TRPL curve at each power. Since the density of photo-excited carriers is proportional to the excitation power, μ also grows with an upper limit, in our case, about 32 at $P = 50P_0$ from the fitting (see the supplementary material, S7). Figure 2(c) exhibits simulated curves with μ obtained from the fitting of Fig. 2(a), and the simulation imitates the corresponding experimental intensity profiles very well, including the prolonged rise time and the temporal shift in the TRPL curves with the power.

To quantitatively characterize the changes in the rise dynamics, we introduce a total retardation time (τ_{ret}) as the time difference between the pulse excitation at $t = 0$ and the time at maximum intensity. From the model in Eq. (1), τ_{ret} occurs at $\tau_M \ln\left(\mu\sqrt{\tau_X/\tau_M}\right)$ and increases logarithmically with μ under fixed τ_x and τ_M. Figure 2(d) plots experimentally measured and calculated τ_{ret} as a function of the excitation power, confirming that τ_{ret} is predictable and controllable with the excitation power.

With the retardation of the single-exciton emission (I_X), a new peak in Fig. 2(a) emerges at $t = 0$ with increasing excitation power, not shown in the simulation curves. In contrast to the single-exciton emission, the new peak does not exhibit any retardation with power. We attribute this peak to the spectrally superimposed cavity emission, as shown in the PL spectrum. To confirm this fact, we separately measured the decay curve at the center of the mode M3 and compared it to the decay curve at $P = 50P_0$ in Fig. 2(a). The decay curve of M3 mode and the new peaks in the TRPL curve at the high excitation power are identical, verifying that the new peak comes from the background cavity emission (I_C). Since the broad cavity emission is mostly fed by the continuum states and multi-exciton states, it does not experience temporal retardation with the excitation power.

This difference in the temporal retardation between I_X and I_C plays a vital role in maintaining the single-photon purity at high excitation power. In general, the background emissions and possible re-excitation at high excitation power increase multi-photon probability, and these emissions cannot be eliminated with spectral and polarization filters. However, the temporally retarded I_X enables us to improve the single-photon purity by temporal decoupling. To examine how the single-photon characteristic changes with the power, we performed second-order photon-correlation

measurements at a 20 MHz excitation laser repetition rate. Figure 3(a) shows the measured antibunching curves at different excitation powers of $P = P_0, 10P_0,$ and $40P_0$ without any subtraction. We separately measured and determined continuous background signals due to a large after-pulse and dark counts of the InGaAs

detectors (see the supplementary material, S8). Figure 3(b) depicts a close-up view of Fig. 3(a) and shows a fine structure in an anti-bunching peak at the center. Such complicated features in the $g^{(2)}(t)$ curve originate from the auto- and cross-correlations of temporally separated I_X and I_C as described in the following equation:

$$g^{(2)}(t) = \frac{\langle : I_X(\tau)I_X(\tau + t) : \rangle + \langle : I_C(\tau)I_C(\tau + t) : \rangle + \langle : I_X(\tau)I_C(\tau + t) : \rangle + \langle : I_C(\tau)I_X(\tau + t) : \rangle}{\langle : I_X + I_C : \rangle^2}. \tag{2}$$

Considering these auto- and cross-correlations of I_X and I_C, we fit the measured $g^{(2)}(t)$ curves (see the supplementary material, S8). At a relatively low power P_0, the auto-correlation signal of I_X is dominant over other signals, resulting in $g^{(2)}(0) = 0.23(0.01)$. Non-zero $g^{(2)}(0)$ would be due to the possible re-excitation of QDs with the 70 ps-long pulse laser and the broad background emissions from hybridized continuum states of nearby QDs and wetting layer. As the excitation power increases much higher than P_0, the background emissions efficiently feed the cavity mode that enlarges the auto-correlation signal of I_C as well as the cross-correlation signal between I_X and I_C. Since there exists temporal separation of τ_{ret} between I_X and I_C, the cross-correlation signals appear at a different delay time from the auto-correlation signals in the $g^{(2)}(t)$ curve. This leads to a double-peak feature of the center peak and temporal broadening of the other peaks at delay times ±50 ns. As τ_{ret} increases with the excitation laser power, the separation of the double peaks at the center also increases with the power.

As expected, the auto- and cross-correlation signals of the strong cavity emission at high excitation power significantly degrade the single-photon purity. However, given the temporal retardation of I_X from I_C by $\tau_{ret} = 4.3$ ns, we can selectively eliminate the I_C-related auto-correlation and cross-correlation signals from

the $g^{(2)}(t)$ curve by temporal filtering of the emissions before τ_{ret}. We verified such a filtering effect on $g^{(2)}(t)$ by measuring the correlation curve in the time-tagged-time-resolved mode, which allows us to selectively collect the signals at a certain time window. Figures 3(c) and 3(d) show the reconstructed $g^{(2)}(t)$ curves at $P = 40P_0$ with different filtering ranges of $0.54R_{ret}$ ($0 < t < 0.54\tau_{ret}$ = 2.3 ns) and R_{ret} ($0 < t < \tau_{ret}$ = 4.3 ns) and their close-up view for the center peak. As the temporal filtering range increases, the $g^{(2)}(0)$ value decreases from initially 0.4 to 0.18 in the filtering range R_{ret}. Increasing the temporal filtering range more than τ_{ret} can improve the $g^{(2)}(0)$ further, but it reduces the brightness of single photons. With the filtering range R_{ret}, we maintain 75% brightness, while increasing the filtering range to $1.5R_{ret}$ yields much lower $g^{(2)}(0) = 0.05(0.02)$ with 45% brightness (see the supplementary material, S9). Therefore, the $g^{(2)}(0)$ at high excitation power could be even lower than that at $P = P_0$ since a few-ns long retardation effectively decouples I_X from the possible background emissions and decreases the probability of re-excitation. These results show that accessing multi-exciton states allows for the engineering of the rise dynamics of single excitons without degrading single-photon purity.
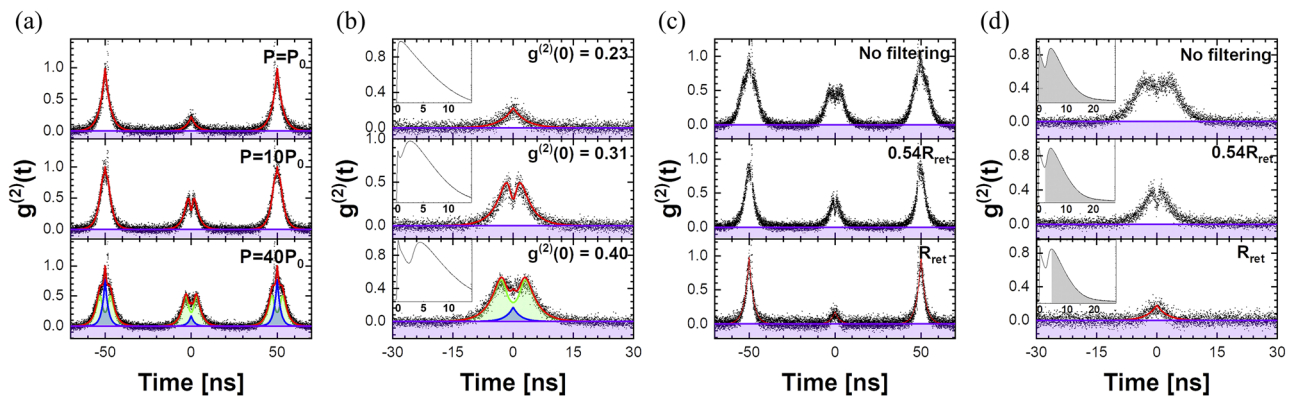

FIG. 3. (a) Second-order intensity correlation curves $g^{(2)}(t)$ of the single exciton at different excitation powers of $P = P_0, 10P_0,$ and $40P_0$ at 4 K. (b) Close-up view of (a) for the center peak, showing a separated double-peak feature at high excitation power. The red lines in (a) and (b) represent fitted curves. The blue and green regions are auto- and cross-correlation parts, respectively. The violet regions are the constant background signals, including the after-pulse signals and the dark counts of InGaAs detectors. The insets in (b) represent the TRPL data at each excitation power. (c) Reconstructed $g^{(2)}(t)$ curves with different filtering ranges at $P = 40P_0$; no filtering (top), $0.54R_{ret}$ ($0 < t < 0.54\tau_{ret}$ = 2.3 ns) (middle), and R_{ret} ($0 < t < \tau_{ret}$ = 4.3 ns) (bottom). (d) Close-up view of (c) for the center peak. The insets show the TRPL data with the recorded time window (gray region).

Although we successfully extended the rise time by more than 1 ns, to match the time scale between the rise and decay times, we additionally modified the decay dynamics by controlling the Purcell effect with N_2 gas.[41,42] At 4 K, the injected N_2 gas encrusts the surface of the $L3$ cavity and red-shifts the cavity mode.[42] Hence, controlling the deposition time of the N_2 gas enables us to change the cavity detuning δ between I_X and the center of the cavity mode. Figure 4(a) displays PL spectra with different cavity detuning δ = 3.03, 2.19, and 0.76 meV at the excitation power $P = 0.5P_0$ and the corresponding TRPL data. By decreasing δ, the decay time reduces from 4.1 ns to 3.0 and 1.3 ns. Considering an average single-exciton lifetime of 1.8(0.6) ns in bulk InP, the observed values correspond to Purcell enhancement of 0.44, 0.6, and 1.4, respectively. At the smallest δ, τ_X decreases as fast as the rise time we achieved at high excitation power. In Fig. 4(b), we compare the temporal profiles before and after modifying the exciton dynamics. Initially, the single-exciton

emission had an asymmetric temporal profile with a fast rise time of 0.2 ns and a slow decay time of 4.1 ns [left, Fig. 4(b)]. As we combine the techniques for multi-exciton cascade recombination and cavity detuning, we extend the rise time [middle, Fig. 4(b)] and shorten the decay time [right, Fig. 4(b)], which demonstrates a symmetrical temporal profile of the I_X. From this modified temporal profile, we calculate 77.9% overlap with a Gaussian function having an FWHM of 2.89 ns [right, Fig. 4(b)]. Reducing the detuning between I_X and I_C can degrade the single-photon purity due to the increased the cavity background emission. However, from a separate experiment, we confirmed that applying temporal filtering in the $1.5R_{ret}$ filtering range at $P = 5P_0$ can lower the $g^{(2)}(0) = 0.46(0.002)$ into 0.34(0.005) with 32% brightness (see the supplementary material, S10).

III. CONCLUSION

In conclusion, we have demonstrated the single-photon pulses with Gaussian spatial and temporal mode profiles from the cavity-integrated QDs. Compared to previous approaches based on the modulation of emission or excitation pulses, our approach directly engineers the exciton dynamics using the multi-exciton cascade recombination process and the Purcell effect. Furthermore, introducing cascade recombination selectively retards single-exciton emissions from possible background emission and reduces the re-excitation. This enables us to recover the purity of single photons at high excitation power.

Together with the purity, indistinguishability is also an important figure of merit of single-photon sources. Non-resonant excitation generally limits the indistinguishability with a short coherence time. However, decoupling the single excitons from such dephasing sources could improve the indistinguishability. For example, InAs/InP QDs have reported a long coherence time over 1 ns even with the above-band excitation by eliminating the wetting layer.[43,44] This long coherence time was possible by spatially separating the excitons from a noisy charge environment. In our approach, the cascade recombination could temporally separate the single excitons from these charge noises. Therefore, investigating the indistinguishability of the temporally retarded single photons from the excitation will be interesting for examining the type of dephasing and their time scales.

Controlling the exciton dynamics can be applied to other photonic structures, such as Bull's eyes[8,45] and photonic wire cavities.[23] These low Q photonic structures have similar Gaussian far-field profiles with moderate enhancement in the spontaneous emission rate. Given such broad adaptability, our approach would bring the capabilities of producing temporal- and spatial-Gaussian single-photon waveforms from QDs.

SUPPLEMENTARY MATERIAL

See the supplementary material for the details of Gaussian temporal shaping using the electro-optic modulator (S1), experimental setup (S2), optical properties of cavity-coupled QD (S3), cavity properties of mode M3 (S4), far-field mode overlap integral (S5), experimental collection efficiency (S6), theoretical model of multi-exciton cascade recombination process (S7), $g^{(2)}(t)$ analysis (S8), brightness and single-photon purity depending on the filtering range (S9), and single-photon purification at small detuning (S10).
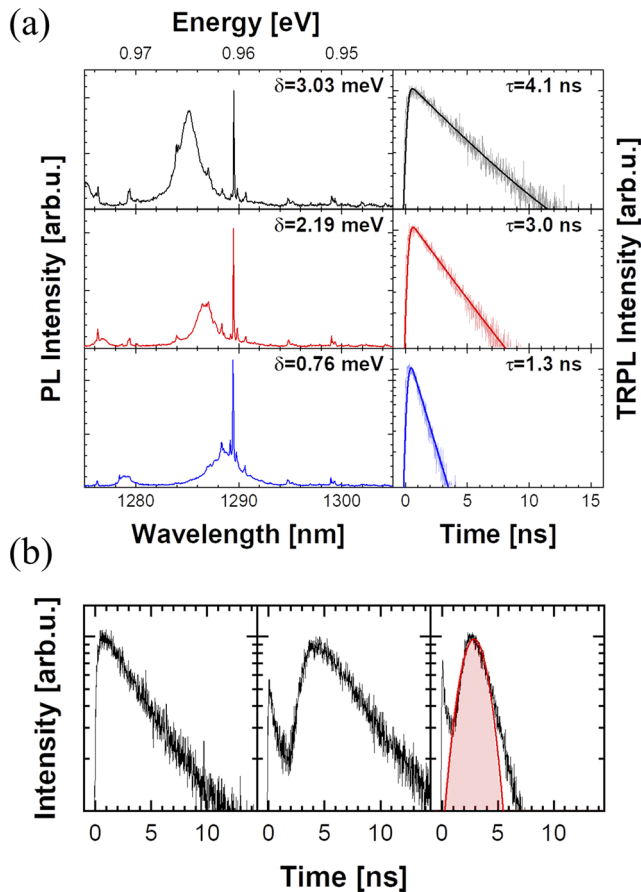

FIG. 4. (a) PL spectra of cavity-coupled QDs with different cavity detuning δ = 3.03 (top), 2.19 (middle), and 0.76 meV (bottom). The corresponding TRPL curves are shown in the right panel. (b) Comparison of the TRPL curves in the typical excitation condition at $P = 0.5P_0$ and δ = 3.03 meV (left), after introducing the multi-exciton cascade recombination at $P = 50P_0$ and δ = 3.03 meV (middle), and additionally enhancing the Purcell effect at $P = 10P_0$ with δ = 0.76 meV (right). The red-shaded area is a fitted Gaussian function with an FWHM of 2.89 ns for comparison.

DATA AVAILABILITY

The data that support the findings of this study are available from the corresponding author upon reasonable request.

REFERENCES

[1] N. Gisin, G. Ribordy, W. Tittel, and H. Zbinden, Rev. Mod. Phys. **74**, 145 (2002).
[2] S.-K. Liao, W.-Q. Cai, W.-Y. Liu, L. Zhang, Y. Li, J.-G. Ren, J. Yin, Q. Shen, Y. Cao, Z.-P. Li *et al.*, Nature **549**, 43 (2017).
[3] S. Pirandola, J. Eisert, C. Weedbrook, A. Furusawa, and S. L. Braunstein, Nat. Photonics **9**, 641 (2015).
[4] L. A. Lugiato, A. Gatti, and E. Brambilla, J. Opt. B **4**, S176 (2002).
[5] A. P. Lund, M. J. Bremner, and T. C. Ralph, NPJ Quantum Inf. **3**, 15 (2017).
[6] F. Arute, K. Arya, R. Babbush, D. Bacon, J. C. Bardin, R. Barends, R. Biswas, S. Boixo, F. G. S. L. Brandao, D. A. Buell *et al.*, Nature **574**, 505 (2019).
[7] T. Müller, J. Skiba-Szymanska, A. B. Krysa, J. Huwer, M. Felle, M. Anderson, R. M. Stevenson, J. Heffernan, D. A. Ritchie, and A. J. Shields, Nat. Commun. **9**, 862 (2018).
[8] H. Wang, H. Hu, T.-H. Chung, J. Qin, X. Yang, J.-P. Li, R.-Z. Liu, H.-S. Zhong, Y.-M. He, X. Ding *et al.*, Phys. Rev. Lett. **122**, 113602 (2019).
[9] J. Liu, R. Su, Y. Wei, B. Yao, S. F. C. da Silva, Y. Yu, J. Iles-Smith, K. Srinivasan, A. Rastelli, J. Li *et al.*, Nat. Nanotechnol. **14**, 586 (2019).
[10] A. Musiał, P. Holewa, P. Wyborski, M. Syperek, A. Kors, J. P. Reithmaier, G. Sęk, and M. Benyoucef, Adv. Quantum Technol. **3**, 1900082 (2020).
[11] E. Meyer-Scott, C. Silberhorn, and A. Migdall, Rev. Sci. Instrum. **91**, 041101 (2020).
[12] M. Toishi, D. Englund, A. Faraon, and J. Vučković, Opt. Express **17**, 14618 (2009).
[13] J. Claudon, J. Bleuse, N. S. Malik, M. Bazin, P. Jaffrennou, N. Gregersen, C. Sauvan, P. Lalanne, and J.-M. Gérard, Nat. Photonics **4**, 174 (2010).
[14] S. Haffouz, K. D. Zeuner, D. Dalacu, P. J. Poole, J. Lapointe, D. Poitras, K. Mnaymneh, X. Wu, M. Couillard, M. Korkusinski *et al.*, Nano Lett. **18**, 3047 (2018).
[15] M. D. Birowosuto, H. Sumikura, S. Matsuo, H. Taniyama, P. J. van Veldhoven, R. Nötzel, and M. Notomi, Sci. Rep. **2**, 321 (2012).
[16] P. Senellart, G. Solomon, and A. White, Nat. Nanotechnol. **12**, 1026 (2017).
[17] S. Hepp, S. Bauer, F. Hornung, M. Schwartz, S. L. Portalupi, M. Jetter, and P. Michler, Opt. Express **26**, 30614 (2018).
[18] S. Sun, H. Kim, G. S. Solomon, and E. Waks, Nat. Nanotechnol. **11**, 539 (2016).
[19] D. Najer, I. Söllner, P. Sekatski, V. Dolique, M. C. Löbl, D. Riedel, R. Schott, S. Starosielec, S. R. Valentin, A. D. Wieck *et al.*, Nature **575**, 622 (2019).
[20] H. Wang, W. Li, X. Jiang, Y.-M. He, Y.-H. Li, X. Ding, M.-C. Chen, J. Qin, C.-Z. Peng, C. Schneider *et al.*, Phys. Rev. Lett. **120**, 230502 (2018).
[21] M. Gimeno-Segovia, T. Rudolph, and S. E. Economou, Phys. Rev. Lett. **123**, 070501 (2019).
[22] Z.-C. Duan, J.-P. Li, J. Qin, Y. Yu, Y.-H. Huo, S. Höfling, C.-Y. Lu, N.-L. Liu, K. Chen, and J.-W. Pan, Opt. Express **28**, 18917 (2020).
[23] M. Munsch, N. S. Malik, E. Dupuy, A. Delga, J. Bleuse, J.-M. Gérard, J. Claudon, N. Gregersen, and J. Mørk, Phys. Rev. Lett. **110**, 177402 (2013).
[24] L. Sapienza, M. Davanço, A. Badolato, and K. Srinivasan, Nat. Commun. **6**, 7833 (2015).
[25] Y. Ma, G. Ballesteros, J. M. Zajac, J. Sun, and B. D. Gerardot, Opt. Lett. **40**, 2373 (2015).
[26] J.-H. Kim, T. Cai, C. J. K. Richardson, R. P. Leavitt, and E. Waks, Optica **3**, 577 (2016).
[27] P. P. Rohde, T. C. Ralph, and M. A. Nielsen, Phys. Rev. A **72**, 052332 (2005).
[28] M. Cao, F. Hoffet, S. Qiu, A. S. Sheremet, and J. Laurat, Optica **7**, 1440 (2020).
[29] K. A. Fischer, K. Müller, K. G. Lagoudakis, and J. Vučković, New J. Phys. **18**, 113053 (2016).
[30] M. T. Rakher and K. Srinivasan, Appl. Phys. Lett. **98**, 211103 (2011).
[31] S. Ates, I. Agha, A. Gulinatti, I. Rech, A. Badolato, and K. Srinivasan, Sci. Rep. **3**, 1397 (2013).
[32] R. P. Leavitt and C. J. K. Richardson, J. Vac. Sci. Technol. B **33**, 051202 (2015).
[33] C. Santori, G. S. Solomon, M. Pelton, and Y. Yamamoto, Phys. Rev. B **65**, 073310 (2002).
[34] D. Elvira, R. Hostein, B. Fain, L. Monniello, A. Michon, G. Beaudoin, R. Braive, I. Robert-Philip, I. Abram, I. Sagnes *et al.*, Phys. Rev. B **84**, 195302 (2011).
[35] M. Winger, T. Volz, G. Tarel, S. Portolan, A. Badolato, K. J. Hennessy, E. L. Hu, A. Beveratos, J. Finley, V. Savona *et al.*, Phys. Rev. Lett. **103**, 207403 (2009).
[36] M. Kaniber, A. Laucht, A. Neumann, J. M. Villas-Bôas, M. Bichler, M.-C. Amann, and J. J. Finley, Phys. Rev. B **77**, 161303 (2008).
[37] K. H. Madsen, S. Ates, J. Liu, A. Javadi, S. M. Albrecht, I. Yeo, S. Stobbe, and P. Lodahl, Phys. Rev. B **90**, 155303 (2014).
[38] R. Ferreira and G. Bastard, Appl. Phys. Lett. **74**, 2818 (1999).
[39] G. A. Narvaez, G. Bester, and A. Zunger, Phys. Rev. B **74**, 075403 (2006).
[40] E. Dekel, D. V. Regelman, D. Gershoni, E. Ehrenfreund, W. V. Schoenfeld, and P. M. Petroff, Solid State Commun. **117**, 395 (2001).
[41] T. Kuroda, N. Ikeda, T. Mano, Y. Sugimoto, T. Ochiai, K. Kuroda, S. Ohkouchi, N. Koguchi, K. Sakoda, and K. Asakawa, Appl. Phys. Lett. **93**, 111103 (2008).
[42] J.-H. Kim, C. J. K. Richardson, R. P. Leavitt, and E. Waks, Nano Lett. **16**, 7061 (2016).
[43] M. Anderson, T. Müller, J. Huwer, J. Skiba-Szymanska, A. B. Krysa, R. M. Stevenson, J. Heffernan, D. A. Ritchie, and A. J. Shields, NPJ Quantum Inf. **6**, 14 (2020).
[44] M. Anderson, T. Müller, J. Skiba-Szymanska, A. B. Krysa, J. Huwer, R. M. Stevenson, J. Heffernan, D. A. Ritchie, and A. J. Shields, Appl. Phys. Lett. **118**, 014003 (2021).
[45] M. Davanço, M. T. Rakher, D. Schuh, A. Badolato, and K. Srinivasan, Appl. Phys. Lett. **99**, 041102 (2011).